Magnetic-circular-dichroism microspectroscopy at the spin reorientation transition in Ni(001) films

W. Kuch, J. Gilles, and S. S. Kang
Max-Planck-Institut für Mikrostrukturphysik, Weinberg 2, D-06120 Halle, Germany

S. Imada and S. Suga
Osaka University, Graduate School of Engineering Science, 1–3 Machikaneyama, Toyonaka 560-8531, Japan

J. Kirschner
Max-Planck-Institut für Mikrostrukturphysik, Weinberg 2, D-06120 Halle, Germany
(Received 10 November 1999)

The spin reorientation transition in fcc Co/Ni/Cu(001) epitaxial ultrathin films as a function of Co and Ni film thickness is studied by the combination of photoelectron emission microscopy and x-ray magnetic-circular-dichroism spectroscopy at the Ni $L_{2,3}$ edge. This microspectroscopic technique allows one to extract local quantitative information about the Ni magnetic properties on a submicrometer scale. Domain images in the thickness range of 1.4–2.6 atomic monolayers (ML) Co and 11–14 ML Ni show that the spin reorientation occurs as a function of both Co and Ni thicknesses. Increasing the Co thickness or decreasing the Ni thickness leads to a switching of the magnetic easy axis from [001] out-of-plane to ⟨110⟩ in-plane directions. A constant effective Ni spin moment similar to the bulk magnetic moment is observed. The Ni orbital to spin moment ratio shows distinctly different values for out-of-plane magnetization (0.080 ± 0.005) and in-plane magnetization (0.053 ± 0.005). This is discussed in terms of the connection to the Ni magnetocrystalline anisotropy. The domain density of the perpendicular magnetization increases towards the spin reorientation transition line.

I. INTRODUCTION

A considerable portion of current research on ultrathin magnetic films is focused on the direction of the easy axis of magnetization. It is determined by the magnetic anisotropy energy (MAE), which in epitaxial thin films contains important thickness-dependent contributions connected to the presence of a surface or interface, or to the elastic strain. The minimum of the sum of the MAE and the magnetostatic demagnetizing energy (shape anisotropy) defines the easy axis of magnetization. Spin reorientation transitions of the easy axis of magnetization in ultrathin films may occur as a function of film thickness, temperature, or composition. Both thin films with a magnetization in the film plane and perpendicular to it have important technological relevance. Therefore measurement and control of the MAE are important technical issues.

The MAE is related to the anisotropy of the orbital magnetic moment, as discussed by Bruno,[1] and later experimentally verified.[2–5] The orbital moment should be higher for a direction of magnetization preferred by the MAE.[6–8] This opens the possibility of determining the angular dependence of the MAE in an element-selective way by measuring the orbital magnetic moment by magnetic circular dichroism in soft x-ray absorption (XMCD). XMCD probes the spin and orbital asymmetry of the unoccupied part of the band structure just above the Fermi level.[9] Transitions of spin- and orbit-polarized core level electrons into the unoccupied part of the exchange split valence bands are excited by circularly polarized x rays. The dichroism, i.e., the difference in absorption intensity upon reversal of helicity, thereby depends on the projection of the direction of the incoming photons onto the magnetization direction. The intensity of photoemitted electrons from a sample surface is most often used as a convenient measure for the absorption.

Sum rules have been proposed to deduce quantitative information from XMCD spectra.[10,11] Although there has been some dispute about the applicability of these rules,[12–15] they seem to yield reasonable results for the $3d$ transition metals.[14–16] These sum rules allow one to extract numbers for the spin and orbital magnetic moments from a comparison of the absorption cross section at the L_3 and L_2 edges of transition metals. They enable thus the separate determination of magnetic properties of different elements in the same sample.

This element specificity has been used by Dürr *et al.* to study element-resolved anisotropies of a stack of three atomic monolayer (ML) Co on top of 30 ML Ni on Cu(001).[4] Epitaxial Ni films on Cu(001) show a spin reorientation transition from an easy axis parallel to the film plane at film thicknesses below $\approx 8-10$ ML to an easy axis perpendicular to the film plane at thicknesses between ≈ 8 ML and 56–75 ML.[17–25] The perpendicular magnetization is attributed to a magnetoelastic contribution to the MAE caused by substrate-induced strain in the epitaxial Ni film.[20–28] The MAE of Co/Cu(001), on the other hand, favors an in-plane easy axis.[29–32] Although the gross magnetization direction is in the plane of the film in 3 ML Co/30 ML Ni/Cu(001), it was possible by using XMCD to prove that the Ni film still maintains its perpendicular MAE.[4] The stronger in-plane anisotropy contribution of the (thinner) Co film, however, redirects the magnetization direction of the entire film to the in-plane direction.

From this competition of Ni perpendicular MAE, Co in-

plane MAE, and (in-plane) magnetostatic energy, it follows that spin reorientation transitions in Co/Ni/Cu(001) can be expected to take place at proper combinations of Ni and Co film thicknesses for which these energy contributions cancel out.[33] The total MAE of the Co/Ni stack may be designed to give a desired value by tuning the Co and Ni film thicknesses. The spin reorientation transitions in Co/Ni double layers are thus ''enforced'' in the sense that the elemental anisotropies of the single constituents do not change their sign between out-of-plane and in-plane magnetization of the entire bilayer. Therefore both the Ni and Co films experience transitions from their respective hard axis to the easy axis of magnetization at the spin reorientation transition and vice versa. The element-resolved MAEs probed by XMCD should consequently exhibit a distinct change in orbital moment at the spin reorientation transition.

The rapidly decreasing size of technologically employed magnetic structures fuels the development of techniques which allow the imaging of magnetic domains on a submicrometer scale. Photoelectron emission microscopy (PEEM) combined with resonant excitation by circularly polarized light is one that has already proved its feasibility for the study of magnetic microstructures and multilayers.[34,35] The lateral intensity distribution of emitted low-energy secondary electrons is magnified by electron lenses. Magnetic contrast is achieved by the XMCD effect: Circularly polarized radiation tuned to elemental absorption edges leads to dichroism in absorption and, hence, to a different secondary electron intensity for domains having different magnetization components along the direction of incoming light. Magnetic domains can then be distinguished in the images by different grayscales corresponding to the secondary electron intensity.

The consequent improvement is to take advantage of the *full* spectroscopic information inherent to XMCD without giving up the spatial resolution of PEEM. This implies scanning the photon energy and recording microscopic images of the secondary electron intensity for both photon helicities at each energy step, not only at the absorption maximum. Local XMCD spectra at any position can be analyzed from such a set of images. Instead of the qualitative information contained in images of magnetic domains obtained at one fixed photon energy, full quantitative information can be extracted from XMCD analysis of such a spectral series of images with the same spatial resolution. With the availability of powerful third-generation synchrotron light sources, the acquisition of such spectral series of absorption images became feasible in a reasonable time. The advantages of both methods, namely, the element-selective quantitative information on electronic and magnetic properties by means of XMCD, and the lateral resolution of PEEM, are combined in this way for performing microspectroscopy.

In this contribution we present an XMCD-PEEM microspectroscopic study of the spin reorientation transition in epitaxial Co/Ni/Cu(001) films. Both Co and Ni layers were prepared as crossed wedges with slopes rotated by 90° with respect to each other. In these samples the spin reorientation transition can be observed as a line separating the regions of in-plane and perpendicular magnetization, determined by the cancellation of Co and Ni MAE and shape anisotropy energy as a function of both layer thicknesses. XMCD spectra at the Ni $L_{2,3}$ edge were recorded for pixels corresponding to 370×370 nm^2 on the sample surface. Sum-rule analysis of these local XMCD spectra is used to present microscopic images of the effective Ni spin magnetic moment in the vicinity of the spin reorientation transition. Analysis with respect to the orbital moment reveals that a distinct jump of the Ni orbital magnetic moment occurs right at the spin reorientation transition, in accordance with an intrinsic Ni elemental MAE favoring out-of-plane magnetization irrespective of the magnetization direction of the whole Co/Ni stack.

II. EXPERIMENT

The measurements were performed at the twin helical undulator beamline for soft x-ray spectroscopy BL25SU of SPring-8 in Japan. Circularly polarized light emitted in the first harmonic from one of the two undulators is monochromatized by a varied spacing plane grating monochromator.[36] After having set the two undulators to opposite helicity, helicity reversal was realized by closing one undulator and fully opening the other, which took about 10 min. The degree of circular polarization is expected to be between 95% and 99%. The light was incident to the sample under a grazing angle of 30° from the surface, with an azimuthal angle of 23° to the [110] axis of the Cu substrate. The entrance and exit slits of the monochromator were set to 290 μm for the measurements presented here, which was enough to illuminate a sufficiently large area on the sample. Since the light spot on the sample is an image of the exit slit, the exit slit setting is not critical, and does not influence the photon flux density or the *local* photon energy resolution. The local energy resolution is estimated to be better than 150 meV, so that the spectra can be regarded as representing mainly the intrinsic line shape of the Ni $L_{2,3}$ absorption. The energy dispersion resulting from having an image of the exit slit on the sample surface was found to be only about 20 meV over the vertical dimension of the images taken here (74 μm). All images were normalized to the electron current measured at the last optical element, a gold-coated refocusing mirror.

The experiments were performed at room temperature in an ultrahigh-vacuum chamber (base pressure 1×10^{-8} Pa in the sample preparation chamber and 2×10^{-8} Pa in the PEEM chamber) equipped with standard facilities for sample preparation and surface characterization. The surface of the Cu(001) single-crystal substrate was prepared and checked by Ar ion bombardment, annealing, Auger electron spectroscopy, and low-energy electron diffraction. Nickel and cobalt films were evaporated at room temperature by electron bombardment from high-purity rods. Deposition rates were 0.3 ML/min for Ni and 0.7 ML/min for Co, while the overall pressure in the chamber did not exceed 2×10^{-8} Pa. The evaporation rates were calibrated before preparation of the wedges for continuous films evaporated under identical conditions by means of the oscillations in the medium-energy electron diffraction intensity recorded during the growth. The accuracy of the film thicknesses cited here is estimated as 10%. The wedge-shaped films were prepared by positioning apertures of 2×0.5 mm^2 in front of the sample, with a distance to the sample surface of 1.5 mm in the case of Ni and 1.1 mm in the case of Co. During deposition the sample and mask assembly was slowly (0.1°/s for Ni, and 0.2°/s for Co) rocked by $\pm6°$ about the long axis of the aperture,

which was set at a 90° different sample azimuth for Ni and Co deposition. The total evaporation time corresponded to 14 ML for Ni and 4 ML for Co. This results in four 320×220 μm^2 (Ni×Co) regions of crossed wedges with slopes of 46 and 18 ML/mm for Ni and Co, respectively.

The setup of the photoemission microscope (Focus IS-PEEM) is identical to that described in previous publications.[35] In short, it consists of a three-lens electrostatic straight optical axis microscope with an integral sample stage and a variable-contrast aperture. The extractor voltage was set to 10.0 kV and the aperture to 70 μm for the measurements presented here, which resulted in a resolution of about 0.5 μm. The projection lens voltages were adjusted to give a field of view of ≈ 95 μm. The magnified image is intensified by a two-stage microchannel plate, and converted into visible light by means of a scintillator crystal. The image is then computer recorded with 12-bit resolution by a Peltier-cooled camera (PCO SensiCam). A 4×4 binning of camera pixels was used for the images presented here. One pixel then corresponded to 0.37×0.37 μm^2 of the sample surface. To reduce the amount of data, the region of interest was limited to a rectangle of 192×200 pixel, or 71×74 μm^2. In this area, Ni and Co thicknesses varied in the ranges 10.7–14 ML and 1.33–2.67 ML, respectively.

Exposure times of 30 s per image were used for the energy scans. A total of 105 images for each helicity were recorded as a function of photon energy. The width of the energy steps in the scans was set to 0.65 eV before the L_3 edge and in between the L_3 and L_2 peaks, 0.26 eV near the L_3 peak, 0.34 eV near the L_2 peak, and 1.4 eV in the post-L_2 region. The helicity was reversed only once after completion of a full energy scan. The total time for acquisition of over 8×10^6 data points took about 2 h and 20 min, which included the moving time of the monochromator for wavelength scanning and the time needed to reverse the helicity. The scans were started 9 h after preparation of the films. Although a considerable contamination by residual gas can be expected at the Co surface after that time, we believe that the influence of gas adsorption on the magnetic and electronic properties of the Ni film capped by the Co layer is of minor importance. Possible impacts on the MAE of the Co/Ni double layer will be discussed in Sec. V.

III. DATA ANALYSIS

Sum-rule analysis of the 76 800 absorption spectra had to be automated. The procedure for that is described as follows: After subtraction of the camera offset, the data were normalized to the mirror current. This gives a normalization to the overall photon flux of the entire light spot. It turned out that an additional correction was necessary to account for differences between the *integral* and the *local* photon flux, caused by the angular distribution of the intensity in the undulator radiation, which is also energy dependent. This is different for the two helicities, since the source is located at different positions for the upstream and downstream undulator. For the measurements presented here the ratio of local to integral photon flux of the downstream undulator, which was set to deliver light of positive helicity (photon spin in light propagation direction), was found to be higher by about 18% than that of the upstream undulator. In addition, the difference between the two undulators depended on the photon energy and the position within the light spot on the sample surface. A correction linear in energy was found to be sufficient to account for that.

This energy-dependent correction factor was determined from fitting a straight line to the ratio of two absorption spectra for opposite helicity while excluding from the fit the peak regions in which the dichroism occurs. This was done separately for all pixels in the image. The correction was found to vary smoothly over the image area. It was between 16% and 18% on the low-energy end of the spectra and between 16% and 21% at the high-energy end. The spectra were then normalized to unity edge jump by adjusting the intensity of the spectra to zero in the pre-edge region and to one in the post-edge region. Saturation effects arising from the finite penetration depth of the x rays at the Ni absorption maxima[37–40] are estimated to have only a minor influence of less than 2% for the spin moments and $<4\%$ for the orbital moments at the angle of light incidence and film thickness used here.[40]

To simplify the automated processing of the spectra, a complete sum-rule analysis, which was done as outlined in Ref. 14 or 41, was performed beforehand on the averaged spectra of 320 pixels, taken from a large domain in the lower half of the image. In particular, a background consisting of two step functions with relative statistical heights of 2/3 and 1/3 at the positions of the L_3 and L_2 absorption maxima, respectively, was subtracted from the spectra in order to obtain the white line intensity. The width of these step functions was chosen as 0.5 eV. We assumed the resulting integral of the helicity-averaged absorption spectra to correspond to 1.4 Ni $3d$ holes, rather than determining the number of holes from comparison to a sample with known moment as suggested in Ref. 41. This number enters linearly in both results for the spin and orbital magnetic moments, and thus cancels if we use their ratio. It was chosen to be the same as in Ref. 4; measurements of Srivastava *et al.* of the white line absorption intensity of Ni/Cu(001) as a function of Ni thickness also suggest a number close to 1.4 for Ni thicknesses above 10 ML.[42] The difference between the absorption spectra for opposite light helicities was corrected for the degree of polarization, which was taken as 97%. Evaluating the spin and orbital magnetic moments by applying the sum rules[10,11] to the proper integral of the difference spectrum and normalizing it to the white line intensity gives for Ni an effective spin magnetic moment $\mu_{S,eff}=(0.32\pm0.015)\mu_B$ and an orbital magnetic moment $\mu_L=(0.045\pm0.01)\mu_B$. The effective spin magnetic moment is the quantity that is obtained from application of the spin sum rule.[11] It includes the spin magnetic moment μ_S, plus a contribution from the magnetic dipole term $\frac{7}{2}T_z$. The latter is zero in the bulk of cubic crystals, but can be of the same magnitude as the orbital moment in ultrathin films.[2] If we identify these spectra as belonging to a perpendicularly magnetized domain, the effective spin moment of the film, corrected for the angle between magnetization direction and light incidence direction, would be $0.32\mu_B/\cos 60°=(0.64\pm0.03)\mu_B$. This value is already slightly higher than the bulk value of the Ni magnetic moment $(0.62\mu_B)$.[43] The errors quoted here represent the statistical significance of the data. An additional systematic error, possibly up to 20%, may be present according to

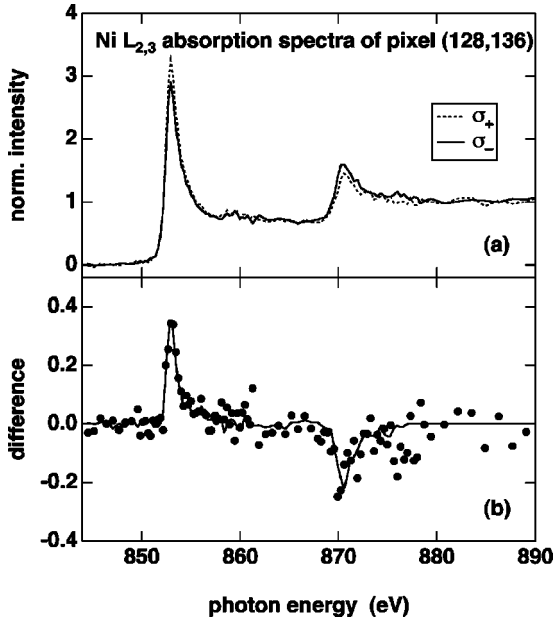

FIG. 1. (a) Ni $L_{2,3}$ absorption spectra of 370×370 nm^2 pixel (128,136). Spectra for positive (negative) helicity are reproduced by dotted (solid) lines. (b) Solid symbols: difference between the two curves of panel (a). Line: template difference spectrum obtained from averaging 320 pixels, shown here with different scaling at the L_3 and the L_2 edge to fit the single-pixel data of pixel (128,136).

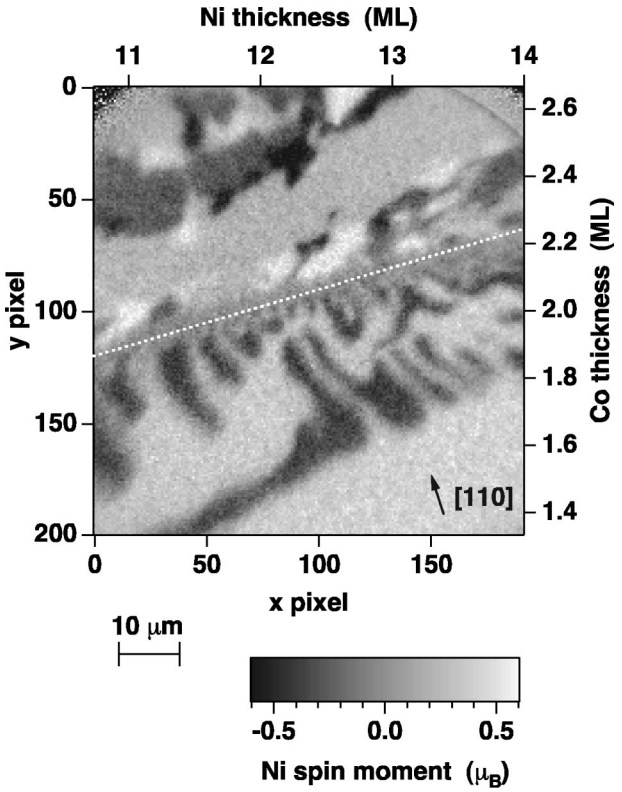

FIG. 2. Result of the pixel-by-pixel sum-rule analysis for the Ni effective spin moment $\mu_{S,eff}$. Different geometrical projections onto the direction of the incident light (from bottom to top, 30° above image plane) are represented by different grayscales, as defined in the legend. Ni and Co thicknesses are given at the top and right axes, respectively. The dotted white line highlights the spin reorientation line which separates regions with out-of-plane magnetization (bottom, two different grayscales) and in-plane magnetization (top, four different grayscales).

the details of background subtraction, the contribution of the magnetic dipole term,[2,7,11,12,44] the number of $3d$ holes, saturation effects, the degree of circular polarization, or the overlap between $2p_{3/2}$ and $2p_{1/2}$ final states.[45] Since the variation of the Ni thickness in the present case is relatively small, we can safely assume that all of the above-mentioned sources of uncertainty in the determination of absolute numbers by the sum rules are virtually constant throughout the range of presented data. They thus do not affect the comparison of moments within the same sample, but have to be kept in mind when discussing the absolute values of the magnetic moments or comparing to literature values.

The XMCD spectra analyzed in this way served as a template for the automated analysis of the single-pixel spectra. The difference curve of the template XMCD spectra was cut into two parts mainly associated with the $2p_{3/2}$ and $2p_{1/2}$ cores, respectively, at 866 eV photon energy. The normalized difference spectra of each pixel were then fitted by that template curve, using only two scaling factors as parameters to fit the two parts. This method was checked to fit the spectra reasonably well over the whole imaged area. Thereby it is assumed that the shape or energetic position of the difference curves is constant. By using only two fit parameters connected to the dichroism intensity at the L_3 and L_2 edges, the fit procedure is very stable, which is a prerequisite for obtaining meaningful information from noisy or scattered single-pixel data. An example is shown in Fig. 1. It shows in the top panel (a) typical absorption spectra of a 0.37×0.37 μm^2 area of the sample for positive and negative helicity (σ_+ and σ_-, respectively). The corresponding dichroism is shown in the bottom panel (b) as the difference between these two curves (solid symbols). The line in Fig. 1(b) is the template difference spectrum, scaled at the L_3 edge by a factor of -0.92 and at the L_2 edge by a factor of -1.60 to fit the single-pixel difference data.

Knowing the area under the L_3 and L_2 peaks of the template difference curve, the respective integrals of the single-pixel curve can be obtained by multiplication with the two fit parameters. It is assumed that the white line intensity of the spectra does not change within the images, being the same as in the template spectra. Some confidence into that assumption is established from checking the height at the L_3 maximum of all of the normalized single-pixel spectra. It varied by less than 5% over the entire image except for its upper edge, where deviations of up to 10% were found. The two degrees of freedom of the fit to the template curve are thus easily converted into the component of spin and orbital moments along the light incidence direction for each pixel of the image.

IV. RESULTS

Figure 2 shows the result for the Ni effective spin moment $\mu_{S,eff}$. The component of $\mu_{S,eff}$ along the direction of the incident light (from bottom to top) is represented in a grayscale, as defined in the legend at the bottom of the image. The Ni and Co thicknesses of the crossed double wedge are given at the top and right axes, respectively. Two distinct

regions with different domain structures are distinguished in Fig. 2, separated by a line that goes from approximately 1.9 ML Co thickness on the left hand side to about 2.2 ML on the right hand side (white dotted line in Fig. 2). Below that line only domains with two different shades of gray, light and dark gray, are found. The average values here are $\pm 0.32\mu_B$. As mentioned before, this is attributed to perpendicularly magnetized domains, belonging to an absolute value of the spin moment of twice that number, $0.64\mu_B$. In the top part of the image, domains with four different grayscales are present. They are seen in Fig. 2 as black, dark gray, bright gray, and white domains. The corresponding values of the effective spin moment are $\pm 0.52\mu_B$ for the black and white and $\pm 0.22\mu_B$ for the dark and bright gray domains. This can be attributed to an in-plane magnetization along four equivalent easy axes along the four $\langle 110 \rangle$ directions. To be able to distinguish all four in-plane magnetization directions, the crystal had been deliberately mounted with an oblique azimuthal incidence angle of $\approx 23°$ with respect to the [110] direction. The projections of the $\pm[110]$ directions onto the incoming light are thus $\pm \cos 30° \cos 23° \approx \pm 0.80$; those of the $\pm[1\bar{1}0]$ are $\pm \cos 30° \cos 67° \approx \pm 0.34$. The image displays thus perpendicularly magnetized domains below the dotted line and domains that are magnetized along easy in-plane $\langle 110 \rangle$ directions on top of that line. The $\mu_{S,eff}$ values of the geometrical projections of the different in-plane and perpendicular domains correspond all to an absolute value of the effective spin moment of Ni of $\approx 0.65\mu_B$. This is slightly higher than the Ni bulk moment of $0.62\mu_B$. As mentioned in Sec. III, however, systematic errors of the order of 20% may be involved in the determination of absolute numbers by sum-rule analysis.

The two regions are separated by a stripe of about 4 μm width, in which the spin reorientation takes place. Its position depends both on the Ni and Co thickness. A spin reorientation from perpendicular to in-plane configuration takes place for decreasing Ni thickness d_{Ni} or increasing Co thickness d_{Co}. The position of the line of the spin reorientation transition can be approximated by $d_{Co} = 0.116 d_{Ni} + 0.62$ ML (d_{Co}, d_{Ni} in ML). The apparent average moment in that stripe is close to zero. Approaching the spin reorientation transition from the perpendicularly magnetized area in the bottom, the average domain size seems to be decreasing. Though it is hard to tell from the present image, the interior of the spin reorientation transition region probably consists of small unresolved domains.

Figure 3 shows, analogously to Fig. 2, the Ni orbital moment of the double wedge. The same domain pattern is recognized although the noise in that image is much higher, especially at the top, where the Ni signal is attenuated by a thicker Co overlayer than at the bottom. The reason for the higher noise in the image of the orbital moment distribution is that the absolute values of the integrals of the L_3 and L_2 dichroism are subtracted in the orbital moment sum-rule analysis, in contrast to the analysis of the spin moment, where they are summed. The worse statistics of the smaller signal and noisier dichroism of the L_2 edge compared to the L_3 edge has thus a much stronger influence on the statistics

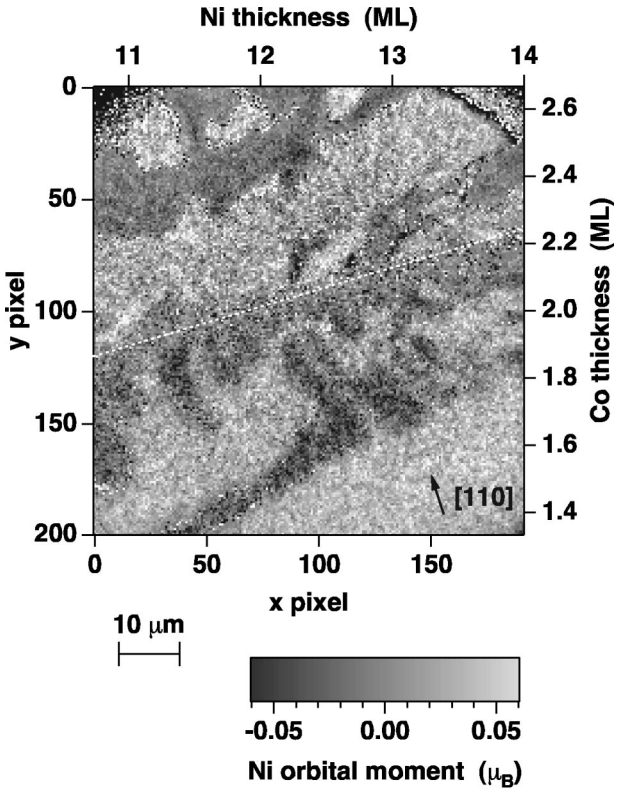

FIG. 3. As Fig. 2, but for the Ni orbital moment μ_L. Different geometrical projections onto the direction of the incident light (from bottom to top, 30° above image plane) are represented by different grayscales, as defined in the legend.

of the orbital moment, where it is close to canceling with the L_3 dichroism.

The interesting quantity for the interpretation of the orbital moment, independent of the magnetization direction, is the ratio of the orbital to spin moment, $\mu_L/\mu_{S,eff}$. Furthermore, assumptions made in the sum-rule analysis concerning the number of d holes, degree of circular polarization, and the determination of the white line intensity do not influence that ratio. However, it is clear from Fig. 3 that the statistics of the present single-pixel data do not allow the pixelwise interpretation in terms of orbital moments. To improve the statistical error in $\mu_L/\mu_{S,eff}$, the information from several pixels has therefore to be averaged. Since we are interested in the behavior of the orbital moment across the spin reorientation transition, averaging of pixels with a common distance from the dotted line has been employed. The result is shown in Fig. 4. Here the orbital to spin moment ratio $\mu_L/\mu_{S,eff}$ is plotted as a function of the distance from the spin reorientation line. The left hand side of Fig. 4 corresponds to the in-plane region of the image, the right hand side to the out-of-plane region. In the center (at the spin reorientation transition) several data points are outside the plot area of Fig. 4 because of division by zero. Each data point contains information of 192 pixels along a line parallel to the spin reorientation transition. $\mu_L/\mu_{S,eff}$ is obtained from the slope of a straight line fit through the origin to a plot of μ_L vs $\mu_{S,eff}$ of these 192 pixels. This way the relative weight of pixels with moments' projections close to zero is automatically reduced.

Although there is considerable scatter, the orbital moment

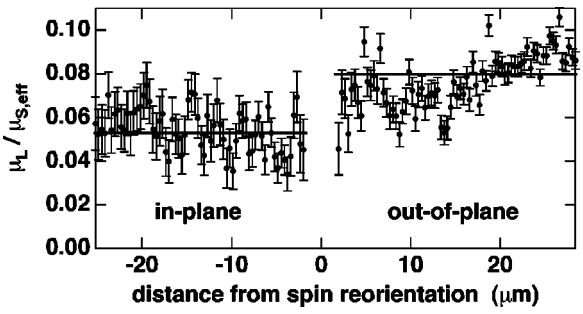

FIG. 4. Orbital to spin moment ratio $\mu_L/\mu_{S,eff}$ as a function of the distance from the spin reorientation line. Each data point is an average of 192 pixels along a line parallel to the spin reorientation transition in Fig. 2. Solid lines mark the average $\mu_L/\mu_{S,eff}$ ratio in the in-plane region (left hand side) and in the out-of-plane region (right hand side).

in the out-of-plane region is seen to be distinctly higher than in the in-plane region by more than $0.02\mu_{S,eff}$. The thick horizontal solid lines in Fig. 4 mark the average $\mu_L/\mu_{S,eff}$ values of the data points that are within the extent of that line. On the in-plane side the average is 0.053 ± 0.005 and on the out-of-plane side 0.080 ± 0.005. In addition, from a look at the data of Fig. 4 one might infer a decreasing trend in the magnitude of the orbital to spin moment ratio towards the spin reorientation transition from both sides. Although the former finding—the sudden change in the orbital moment at the spin reorientation—can be clearly stated, the latter is close to the statistical error. Similar averaging line scans parallel to the spin reorientation line for both perpendicular and in-plane magnetization did not show any such systematic trend. We thus conclude that the orbital moment is approximately constant on both sides of the spin reorientation, but shows distinctly different values for in-plane and out-of-plane magnetization.

V. DISCUSSION

From the position of the spin reorientation line in the two-dimensional d_{Ni}, d_{Co} space of Fig. 2, several statements about the contributing anisotropy energy terms can be made. The energy difference of in-plane magnetization minus out-of-plane magnetization may be written as

$$E(d_{Ni},d_{Co}) = K_{Ni}(d_{Ni}) + K_{Co}(d_{Co}) - \frac{1}{2}\mu_0(M_{Ni}^2 d_{Ni} + M_{Co}^2 d_{Co}), \qquad (1)$$

where K_{Ni}, K_{Co} denote the differences in the MAE between the in-plane and out-of-plane magnetization for the Ni and Co layer, respectively, with $\mu_0 = 4\pi\times10^{-7}$ V s A^{-1}m^{-1} and M_{Ni}, M_{Co} saturation magnetizations per unit volume. The last two terms describe the magnetostatic demagnetizing energy. $E(d_{Ni},d_{Co})=0$ at the spin reorientation. It is obvious from the tilt of the reorientation line (dotted line in Fig. 2) that $K_{Ni}(d_{Ni})$ increases with increasing d_{Ni} and that $K_{Co}(d_{Co})$ decreases with increasing d_{Co}. A linear behavior is often assumed to simplify the thickness dependence of K_{Ni}, K_{Co}:

$$K_{Ni}(d_{Ni}) = K_{Ni}^b d_{Ni} + K_{Ni}^s,$$

$$K_{Co}(d_{Co}) = K_{Co}^b d_{Co} + K_{Co}^s. \qquad (2)$$

In order to follow the usual interpretation of K^b and K^s as bulk and interface anisotropies, for each film the contributions from both interfaces have to be summed, and the common interface between Ni and Co has to be equally divided onto K_{Ni}^s and K_{Co}^s. Although the Co thicknesses in the present case are clearly too low for a separation into bulk and surface terms, we use the linear approximation of Eq. (2) for the sake of (limited) comparison with published literature values.

As mentioned in Sec. IV, the condition $E(d_{Ni},d_{Co})=0$ is approximately fulfilled for $d_{Co}=\alpha d_{Ni}+d_0$, where $\alpha = 0.115\pm0.015$ and $d_0=(0.62\pm0.18)$ ML. Inserting that into Eq. (1), both of the coefficients for the thickness-dependent and the thickness-independent parts of E have to be zero. From the thickness-dependent coefficients, a relationship between K_{Ni}^b and K_{Co}^b is established:

$$-\frac{K_{Ni}^b - \frac{1}{2}\mu_0 M_{Ni}^2}{K_{Co}^b - \frac{1}{2}\mu_0 M_{Co}^2} = \alpha. \qquad (3)$$

Using bulk moments[43] and atomic volumes for epitaxial Co/Cu(001) (Ref. 46) and Ni/Cu(001) (Refs. 47 and 48) films, one gets $\frac{1}{2}\mu_0 M_{Co}^2 = 87.0$ μeV/atom and $\frac{1}{2}\mu_0 M_{Ni}^2 = 11.6$ μeV/atom. Putting these values into Eq. (3), one obtains the result $K_{Co}^b = (190\pm25)$ μeV$-(8.6\pm1.1)K_{Ni}^b$. This links the thickness-dependent part of the Ni MAE to the thickness-dependent part of the Co MAE in order to reproduce the experimentally observed slope of the reorientation line.

It has been discussed in the literature that the perpendicular anisotropy of Ni films on Cu(001) arises from a thickness-dependent magnetoelastic contribution to the MAE,[20,21,23–25,27,28] i.e., $K_{Ni}^b>0$. The MAEs of both pure Ni and Co films on Cu(001) have been measured already previously by conventional techniques. Values of $K_{Ni}^b = +24$ μeV/atom,[21] $+30$ μeV/atom,[20] $+34$ μeV/atom,[23] and $+38$ μeV/atom (Ref. 26) are reported in the literature, obtained from ferromagnetic resonance measurements[20,21,23] and magnetic Kerr effect measurements.[26] The corresponding values for K_{Co}^b using Eq. (3) are then calculated to lie between ≈-20 and -140 μeV/atom. This agrees well with values found in literature, which range from -16 μeV/atom (Ref. 29) over -77 μeV/atom (Ref. 31) to -320 μeV/atom.[30] The slope α of the transition line in Fig. 2 is thus explained by the ratio of Co and Ni effective anisotropies [Eq. (3)].

The extrapolated intersection d_0 of the spin reorientation line with the $d_{Ni}=0$ line is somewhat more difficult to discuss, not only because the error related to d_0 is much bigger than the error in α, but also because the separation into bulk and interface properties for Co is problematic at very low thicknesses, where the Co films may not even be completely closed. From the thickness-independent coefficients of Eq. (1) follows

$$K^s_{Ni}+K^s_{Co}=\left(\frac{1}{2}\mu_0 M^2_{Co}-K^b_{Co}\right)d_0. \quad (4)$$

This allows one to estimate the thickness-independent part of the MAE, $K^s_{Ni}+K^s_{Co}$, to be between $+50$ and $+150$ μeV/(surface atom). Negative interface anisotropies have been reported in the literature for the Ni-Cu interface [-163 μeV/(surface atom),[26] -65 μeV/(surface atom),[18] or -83 μeV/(surface atom) (Ref. 19)] and the vacuum-Co interface [-420 μeV/(surface atom) (Ref. 29)]. Under the assumption that the vacuum-Co and Ni-Cu interface contributions in Co/Ni/Cu(001) are the same as the above-mentioned literature values of Co/Cu(001) and Cu/Ni/Cu(001), respectively, the MAE connected to the Co-Ni interface has to be relatively high and positive. A previously published value is $+94$ μeV/(surface atom).[30] If we assume the above-mentioned literature values to be relevant in our film, the Co-Ni interface contribution would have to be of the order of $+500$ μeV/(surface atom) to lead to a positive value of $K^s_{Ni}+K^s_{Co}$.

It is known from scanning tunneling microscopy that room-temperature-grown Ni/Cu(001) films become increasingly rough with thickness.[49] However, only a small effect of roughness on the Ni-vacuum interface anisotropy has been found.[50] We have to recall at that point that the measurements were made more than 9 h after the preparation of the Co/Ni layer. Contamination by residual gas adsorption is most likely to influence the vacuum-Co interface. Surface contamination can be expected to drastically decrease the absolute value of the vacuum-Co interface contribution to the MAE, and could also lower M_{Co} to some extent for the Co film thicknesses imaged here. Both terms energetically favor the out-of-plane magnetization. We have indeed observed in Co/Ni crossed wedges that the spin reorientation line moved towards higher Co thicknesses as a function of time; i.e., $E(d_{Ni},d_{Co})$ is becoming more positive with time, namely, with increasing contamination. This could also account for a discrepancy between the present data and those of Ref. 18. There, 2 ML Co has been found to be sufficient to pull the magnetization of an underlying Ni film into the film plane in the complete thickness range between 0 and 18 ML, whereas out-of-plane magnetization is observed in our data between $\approx$13 and 14 ML Ni and 2 ML Co (cf. Fig. 2).

Taking the large scatter in published anisotropy values and the relatively large error into account in the determination of d_0, it is wise to draw only qualitative conclusions about the surface and interface contributions to the total MAE from the present data. Altogether, the positive value of the sum of the thickness-independent terms ($K^s_{Ni}+K^s_{Co}$) is probably the result of a large positive Co-Ni interface contribution. It overcompensates the negative contribution from the Ni-Cu interface and the possibly remaining small negative anisotropy from the Co surface. The ratio between the thickness-dependent MAEs of Ni and Co is in good agreement with values for other epitaxial Co and Ni ultrathin film systems on Cu(001) from the literature.

Besides the above statements about the magnetic anisotropy energies, quantitative PEEM-XMCD microspectroscopy at the Ni $L_{2,3}$ edge allows one to extract position-dependent element-resolved magnetic information concerning spin and orbital moments. The absolute value of the Ni effective spin moment is found to be about constant over the whole image, with roughly the value of the Ni bulk moment. This is in agreement with Ref. 51, where a Ni spin moment of $0.6\mu_B$ in the center layers of Ni/Cu(001) was calculated, while an enhanced moment of $0.73\mu_B$ was predicted for the surface layer. A strongly reduced moment, as found in Cu/Ni/Cu/Si(001) ($0.1\mu_B$ at 30 Å Ni film thickness),[52] can be excluded. This could be an effect related to the different substrate. Previous XMCD measurements of 28 ML Ni/Cu(001), by contrast, yielded even a spin moment as large as $1.2\mu_B$.[38]

The behavior of the ratio of orbital to spin moment across the spin reorientation transition (Fig. 4) is most interesting. It is very likely connected to the Ni magnetocrystalline anisotropy K_{Ni}, which according to the above discussion is positive over the whole range of the image. That means that for the Ni layer the easy axis of magnetization is out of plane. In the upper part of the image the magnetization direction is consequently along hard in-plane directions with respect to the Ni MAE, in the lower part along easy out-of-plane directions. The latter seems to be connected to a distinctly higher orbital to spin moment ratio. This confirms the connection of orbital moment anisotropy and magnetocrystalline anisotropy. According to Bruno[1] there should be a proportionality between the orbital moment difference $\Delta\mu_L$ for out-of-plane and in-plane magnetization and the MAE:

$$K_{Ni}=-\frac{\xi}{4}\frac{G}{H}\frac{\Delta\mu_L}{\mu_B}. \quad (5)$$

ξ is the spin-orbit coupling parameter, which for Ni is about 50 (Ref. 47) to 100 meV (Ref. 53), and G and H are density-of-states integrals.[1] $G/H=1$ only if the exchange splitting is larger than the bandwidth. For transition metals, a rough estimate for G/H is 0.2 or smaller,[2] leading to a proportionality factor between $\Delta\mu_L$ and the MAE of about -2.5–5 meV/μ_B. It was pointed out later by van der Laan that Eq. (5) is only approximately true for the case of a completely filled majority spin band.[8] For Ni, though, this can be assumed to be the case. In Ref. 4 a much higher proportionality factor of ≈ -17 meV/μ_B was calculated for Ni. Another calculation of Hjortstam *et al.* yielded a factor of ≈ -18 or ≈ -26 meV/μ_B, depending on whether the orbital polarization correction is included or not.[27] According to the value we use, the difference between our measured orbital moments for out-of-plane and in-plane magnetization $\Delta\mu_L=(\mu_{L,\perp}/\mu_{S,eff}-\mu_{L,\parallel}/\mu_{S,eff})\mu_{S,eff}=(0.080-0.053)\times 0.65\mu_B=(0.018\pm 0.004)\mu_B$ corresponds to an MAE of either ≈ 60 μeV/atom (for -3 meV/μ_B) or ≈ 300 μeV/atom (for -17 meV/μ_B).

For the interpretation of our data we have assumed here that the influence of changes in the magnetic dipole term T_z on the effective spin moment $\mu_{S,eff}=\mu_S-\frac{7}{2}T_z$ is small. In fact it has been observed that the magnetic dipole term $\frac{7}{2}T_z$ is of the same magnitude as the orbital moment,[2] so that the observed changes in $\mu_L/\mu_{S,eff}$ (cf. Fig. 4) can be considered as mainly representing the changes in μ_L. For $3d$ metals like Ni it is furthermore expected that MAE contributions related to T_z are much weaker than contributions due to the

orbital moment.[8] Experimentally we did not observe a significant difference in $\mu_{S,eff}$ between in-plane and out-of-plane magnetization.

The value of 60 μeV/atom for the MAE agrees in magnitude with the above-discussed thickness-dependent literature MAE values for Ni/Cu(001) films.[20,21,23,26] Here 300 μeV/atom, though, would be a factor of 5 too high. In comparing to anisotropy energies, however, one has to keep in mind that the orbital moments measured by XMCD represent a depth-weighted average over the probing depth of the secondary electrons (about 25 Å for Ni).[40] The highly positive contribution to the MAE of the Co-Ni interface could lead to a higher orbital moment anisotropy in the top Ni layers with respect to lower layers and, consequently, to a higher value of $\Delta\mu_L$. In 13 ML Ni, the exponential attenuation of the secondary electron signal leads to a contribution of 1.45/13 from the topmost atomic layer and to a contribution of 0.65/13 from the bottommost layer. Thus, for example, a $+200$ μeV/surface atom Co-Ni interface anisotropy confined to the top layer and a 30-μeV/atom-volume MAE distributed evenly over the film would be observed as 70 μeV/atom. Moreover, the depth distribution of magnetic anisotropy, which is phenomenologically described by a linear dependence on thickness, is not known.

In an XMCD study of 3 ML Co/33 ML Ni/Cu(001), Dürr *et al.* found an even higher orbital moment anisotropy for Ni.[4] Their value, measured in a transverse geometry, corresponds to an orbital moment difference of $(0.028 \pm 0.014)\mu_B$.[7] Calculations of Hjortstam *et al.*, by contrast, gave orbital moment differences of $0.006\mu_B$ or $0.004\mu_B$ for calculations with and without an orbital polarization correction, respectively,[27] taking a tetragonal distortion of $c/a = 0.94$. Their absolute value for the angle-averaged orbital moment $(\mu_L^{\perp} + 2\mu_L^{\parallel})/3$ at that distortion without orbital polarization is $0.047\mu_B$, which is quite close to our experimental value $(0.08 + 2 \times 0.053) \times 0.65\mu_B/3 = 0.04\mu_B$. Including orbital polarization they arrive at $0.064\mu_B$.[27]

All in all, a low proportionality constant $K_{Ni}/\Delta\mu_L$ of about -4 meV/μ_B is required for an agreement of our experimental data with the expected Ni MAE. It is clear that the uncertainties in this constant do at present not allow conclusions on the exact size of the MAE from XMCD measurements. Ultimate quantitative insight into the relation between magnetocrystalline anisotropy and orbital moment anisotropy will depend on further detailed theoretical studies. However, the measured anisotropy of the orbital moment is qualitatively well accounted for by the behavior of the magnetic anisotropy.

As the last point to discuss, the domain configuration close to the spin reorientation transition is left. The basic features seen in Fig. 2, i.e., a decreasing domain size on the perpendicular side of the reorientation and a distinct stripe in which no clear in-plane or out-of-plane magnetization is visible, resemble those of spin reorientations imaged in Co/Au(111) wedges.[54,55] (Note that in our study the spin reorientation happens as a function of two independent parameters, the Ni and Co film thicknesses in the crossed double wedge, in contrast to these earlier reports.) Films exhibiting a perpendicular anisotropy can lower the magnetostatic energy by the formation of alternatingly up and down magnetized domains.[56] Analytic calculations for the average domain size in such systems revealed a dependence on the film thickness and, more prominently, on the domain wall energy.[57,58] As the latter is reduced by the reduction of the effective anisotropy energy $E(d_{Ni}, d_{Co})$ upon approaching the spin reorientation transition, smaller domains become energetically more favorable. This explains well the experimentally observed decrease of domain size as approaching the spin reorientation transition.[54,59] In our study on Co/Ni/Cu(001) we also see this striking dependence of domain size of the perpendicularly magnetized domains on the distance from the spin reorientation line (lower part of Fig. 2). Alternatingly up and down magnetized stripe domains, oriented perpendicularly to this line, are formed. Closer to the spin reorientation transition they split into smaller stripes, thus reducing the average domain width. We interpret this behavior in accordance with the above-mentioned studies by the balance of magnetostatic energy reduction by stripe domain formation and the cost of domain wall energy necessary to create these domains.

VI. SUMMARY

We have used the combination of XMCD and PEEM in a study of the thickness-dependent spin reorientation transition in ultrathin epitaxial Co/Ni/Cu(001) films. This full-image microspectroscopic technique allows one to obtain quantitative magnetic information with microscopic spatial resolution at any position of an image. Looking at the spin reorientation transition in crossed double wedges of Co and Ni results in images where the transition from in plane to out of plane magnetization direction can be followed in two-dimensional thickness space. The easy axis of magnetization switches from in plane at lower Ni thicknesses or higher Co thicknesses to out of plane at higher Ni thicknesses or lower Co thicknesses. The condition for zero MAE difference between in-plane and out-of-plane magnetization can be approximated by a linear dependence on both thicknesses. From this we deduce the relative size of the Co and Ni thickness-dependent (''bulk'') MAE and the double-layer thickness-independent (''surface'') MAE. Both are in good agreement with values found in literature.

Pixel-by-pixel sum-rule analysis of the images results in images displaying the Ni spin and orbital magnetic moments, projected onto the propagation direction of the illuminating x rays. The Ni effective spin moment is constant with an absolute value of $\approx 0.65\mu_B$. The orbital moment is distinctly higher for out-of-plane magnetization than for in-plane magnetization. We interpret this difference as reflecting the Ni MAE, which leads to an anisotropy in the orbital moment with respect to the magnetization direction. The Ni MAE favors perpendicular magnetization for all thicknesses, so that in-plane and out-of-plane magnetization directions of the Co/Ni bilayer represent hard and easy axes for the Ni layer, respectively.

The formation of perpendicularly magnetized domains with decreasing size upon approaching the spin reorientation transition can be explained by magnetostatic stray field energy minimization for decreasing domain wall energy. XMCD-PEEM microspectroscopic studies with improved lateral resolution will have the potential to investigate magnetic moments in very small domains and even in domain

walls. Such experiments will help us to elucidate the detailed mechanism of the spin reorientation transition in the Co/Ni/Cu(001) system and deliver valuable experimental information in the field of micromagnetics.

Note added in proof. Recently, an article by F. Wilhelm *et al.* was published [Phys. Rev. B **61**, 8647 (2000)] in which the proportionality constant of our Eq. (5), $K_{\mathrm{Ni}}/\Delta\mu_L$, was experimentally determined for Ni in Ni/Pt multilayers as 2.6 meV/μ_B. This value fully supports our discussion.

ACKNOWLEDGMENTS

Financial support by the German Minister for Education and Research (BMBF) under Grant No. 05 SL8EF1 9 and by the Japan Society for Promotion of Science (JSPS) is gratefully acknowledged. We thank the Deutsche Forschungsgemeinschaft (DFG) for financing transportation of the equipment and traveling to Japan under Grant Nos. Ki 358/3-1 and 446 JAP-113/179/0. We would like to thank P. Bruno, R. Frömter, and H. P. Oepen for fruitful discussions, and B. Zada for technical assistance. The synchrotron radiation experiments were performed at SPring-8 with the approval and financial support of the Japan Synchrotron Radiation Research Institute (JASRI) (Proposal No. 1999A0319-NS-np). Our special thanks is for the SPring-8 staff, particularly Y. Saitoh and R.-J. Jung, for generous help during the beam time.

[1] P. Bruno, Phys. Rev. B **39**, 865 (1989).
[2] D. Weller, J. Stöhr, R. Nakajima, A. Carl, M. G. Samant, C. Chappert, R. Mégy, P. Beauvillain, P. Veillet, and G. A. Held, Phys. Rev. Lett. **75**, 3752 (1995).
[3] H. A. Dürr and G. van der Laan, J. Appl. Phys. **81**, 5355 (1997).
[4] H. A. Dürr, G. Y. Guo, G. van der Laan, J. Lee, G. Lauhoff, and J. A. C. Bland, Science **277**, 213 (1997).
[5] D. Weller, Y. Wu, J. Stöhr, M. G. Samant, B. D. Hermsmeier, and C. Chappert, Phys. Rev. B **49**, 12 888 (1994); H. A. Dürr, G. van der Laan, J. Vogel, M. Finazzi, and J. B. Goedkoop, IEEE Trans. Magn. **MAG-34**, 1201 (1998).
[6] J. Stöhr and H. König, Phys. Rev. Lett. **75**, 3748 (1995).
[7] H. A. Dürr and G. van der Laan, Phys. Rev. B **54**, R760 (1996).
[8] G. van der Laan, J. Phys.: Condens. Matter **10**, 3239 (1998).
[9] J. L. Erskine and E. A. Stern, Phys. Rev. B **12**, 5016 (1975); G. Schütz, W. Wagner, W. Wilhelm, P. Kienle, R. Zeller, R. Frahm, and G. Materlik, Phys. Rev. Lett. **58**, 737 (1987).
[10] B. T. Thole, P. Carra, F. Sette, and G. van der Laan, Phys. Rev. Lett. **68**, 1943 (1992).
[11] P. Carra, B. T. Thole, M. Altarelli, and X. Wang, Phys. Rev. Lett. **70**, 694 (1993).
[12] R. Wu and A. J. Freeman, Phys. Rev. Lett. **73**, 1994 (1994).
[13] W. L. O'Brien, B. P. Tonner, G. R. Harp, and S. S. P. Parkin, J. Appl. Phys. **76**, 6462 (1994); D. Rioux, B. Allen, H. Höchst, D. Zhao, and D. L. Huber, Phys. Rev. B **56**, 753 (1997).
[14] C. T. Chen, Y. U. Idzerda, H.-J. Lin, N. V. Smith, G. Meigs, E. Chaban, G. H. Ho, E. Pellegrin, and F. Sette, Phys. Rev. Lett. **75**, 152 (1995).
[15] Y. U. Idzerda, C. T. Chen, H.-J. Lin, H. Tjeng, and G. Meigs, Physica B **208–209**, 746 (1995).
[16] J. Vogel and M. Sacchi, Phys. Rev. B **49**, 3230 (1994); X. Le Cann, C. Boeglin, B. Carrière, and K. Hricovini, *ibid.* **54**, 373 (1996); J. Hunter Dunn, D. Arvanitis, and N. Mårtensson, *ibid.* **54**, R11 157 (1996).
[17] F. Huang, M. T. Kief, G. J. Mankey, and R. F. Willis, Phys. Rev. B **49**, 3962 (1994); W. L. O'Brien and B. P. Tonner, *ibid.* **49**, 15 370 (1994).
[18] W. L. O'Brien, T. Droubay, and B. P. Tonner, Phys. Rev. B **54**, 9297 (1996).
[19] R. Vollmer, T. Gutjahr-Löser, J. Kirschner, S. van Dijken, and B. Poelsema, Phys. Rev. B **60**, 6277 (1999).
[20] B. Schulz and K. Baberschke, Phys. Rev. B **50**, 13 467 (1994).
[21] B. Schulz, R. Schwarzwald, and K. Baberschke, Surf. Sci. **307–309**, 1102 (1994).
[22] G. Bochi, C. A. Ballentine, H. E. Inglefield, C. V. Thompson, R. C. O'Handley, H. J. Hug, B. Stiefel, A. Moser, and H.-J. Güntherodt, Phys. Rev. B **52**, 7311 (1995).
[23] M. Farle, B. Mirwald-Schulz, A. N. Anisimov, W. Platow, and K. Baberschke, Phys. Rev. B **55**, 3708 (1997).
[24] M. Farle, W. Platow, A. N. Anisimov, P. Poulopoulos, and K. Baberschke, Phys. Rev. B **56**, 5100 (1997).
[25] M. Farle, A. N. Anisimov, W. Platow, P. Poulopoulos, and K. Baberschke, J. Magn. Magn. Mater. **198–199**, 325 (1999).
[26] R. Jungblut, M. T. Johnson, J. aan de Stegge, A. Reinders, and F. J. A. den Broeder, J. Appl. Phys. **75**, 6424 (1994).
[27] O. Hjortstam, K. Baberschke, J. M. Wills, B. Johansson, and O. Eriksson, Phys. Rev. B **55**, 15 026 (1997).
[28] C. Uiberacker, J. Zabloudil, P. Weinberger, L. Szunyogh, and C. Sommers, Phys. Rev. Lett. **82**, 1289 (1999); G. Y. Guo, J. Magn. Magn. Mater. **176**, 97 (1997).
[29] P. Krams, F. Lauks, R. L. Stamps, B. Hillebrands, and G. Güntherodt, Phys. Rev. Lett. **69**, 3674 (1992).
[30] M. T. Johnson, J. J. de Vries, N. W. E. McGee, J. aan de Stegge, and F. J. A. den Broeder, Phys. Rev. Lett. **69**, 3575 (1992).
[31] M. Kowalewski, C. M. Schneider, and B. Heinrich, Phys. Rev. B **47**, 8748 (1993).
[32] C. M. Schneider, A. K. Schmid, P. Schuster, H. P. Oepen, and J. Kirschner, in *Magnetism and Structure in Systems of Reduced Dimension*, edited by R. F. C. Farrow, B. Dieny, M. Donath, A. Fert, and B. D. Hermsmeier (Plenum, New York, 1993); E. Navas, P. Schuster, C. M. Schneider, J. Kirschner, A. Cebollada, C. Ocal, R. Miranda, J. Cerdá, and P. de Andrés, J. Magn. Magn. Mater. **121**, 65 (1993); W. Weber, A. Bischof, R. Allenspach, C. H. Back, J. Fassbender, U. May, B. Schirmer, R. M. Jungblut, G. Güntherodt, and B. Hillebrands, Phys. Rev. B **54**, 4075 (1996); W. Weber, R. Allenspach, and A. Bischof, Appl. Phys. Lett. **70**, 520 (1997).
[33] J. Lee, G. Lauhoff, and J. A. C. Bland, Phys. Rev. B **56**, R5728 (1997); G. Lauhoff, J. Lee, J. A. C. Bland, J. P. Schillé, and G. van der Laan, J. Magn. Magn. Mater. **177-181**, 1253 (1998).
[34] J. Stöhr, Y. Wu, M. G. Samant, B. B. Hermsmeier, G. Harp, S. Koranda, D. Dunham, and B. P. Tonner, Science **259**, 658 (1993); J. Stöhr, H. A. Padmore, S. Anders, T. Stammler, and M. R. Scheinfein, Surf. Rev. Lett. **5**, 1297 (1998).

[35] W. Swiech, G. H. Fecher, Ch. Ziethen, O. Schmidt, G. Schönhense, K. Grzelakowski, C. M. Schneider, R. Frömter, H. P. Oepen, and J. Kirschner, J. Electron Spectrosc. Relat. Phenom. **84**, 171 (1997); C. M. Schneider, J. Magn. Magn. Mater. **175**, 160 (1997); W. Kuch, R. Frömter, J. Gilles, D. Hartmann, Ch. Ziethen, C. M. Schneider, G. Schönhense, W. Swiech, and J. Kirschner, Surf. Rev. Lett. **5**, 1241 (1998).

[36] Y. Saitoh, T. Nakatani, T. Matsushita, T. Miyahara, M. Fujisawa, K. Soda, T. Muro, S. Ueda, H. Harada, A. Sekiyama, S. Imada, H. Daimon, and S. Suga, J. Synchrotron Radiat. **5**, 542 (1998).

[37] W. L. O'Brien and B. P. Tonner, Phys. Rev. B **50**, 2963 (1994).

[38] J. Hunter Dunn, D. Arvanitis, N. Mårtensson, M. Tischer, F. May, M. Russo, and K. Baberschke, J. Phys.: Condens. Matter **7**, 1111 (1995).

[39] V. Chakarian, Y. U. Idzerda, and C. T. Chen, Phys. Rev. B **57**, 5312 (1998).

[40] R. Nakajima, J. Stöhr, and Y. U. Idzerda, Phys. Rev. B **59**, 6421 (1999).

[41] J. Stöhr, J. Electron Spectrosc. Relat. Phenom. **75**, 253 (1995).

[42] P. Srivastava, N. Haack, H. Wende, R. Chauvistré, and K. Baberschke, Phys. Rev. B **56**, R4398 (1997).

[43] E. P. Wohlfahrt, in *Ferromagnetic Materials*, edited by E. P. Wohlfahrt (North-Holland, Amsterdam, 1980), Vol. 1.

[44] C. F. J. Flipse, J. J. de Vries, G. van der Laan, M. Surman, A. Partridge, and W. J. M. de Jonge, J. Magn. Magn. Mater. **148**, 141 (1995); G. van der Laan and H. A. Dürr, Physica B **248**, 121 (1998).

[45] Y. Teramura, A. Tanaka, and T. Jo, J. Phys. Soc. Jpn. **65**, 1053 (1996).

[46] J. R. Cerdá, P. L. de Andres, A. Cebollada, R. Miranda, E. Navas, P. Schuster, C. M. Schneider, and J. Kirschner, J. Phys.: Condens. Matter **5**, 2055 (1993).

[47] W. Kuch, A. Dittschar, K. Meinel, M. Zharnikov, C. M. Schneider, J. Kirschner, J. Henk, and R. Feder, Phys. Rev. B **53**, 11 621 (1996).

[48] W. Platow, U. Bovensiepen, P. Poulopoulos, M. Farle, K. Baberschke, L. Hammer, S. Walter, S. Müller, and K. Heinz, Phys. Rev. B **59**, 12 641 (1999).

[49] J. Shen, J. Giergiel, and J. Kirschner, Phys. Rev. B **52**, 8454 (1995).

[50] P. Poulopoulos, J. Lindner, M. Farle, and K. Baberschke, Surf. Sci. **437**, 277 (1999).

[51] O. Hjortstam, J. Trygg, J. M. Wills, B. Johansson, and O. Eriksson, Phys. Rev. B **53**, 9204 (1996).

[52] S. Hope, J. Lee, P. Rosenbusch, G. Lauhoff, J. A. C. Bland, A. Ercole, D. Bucknall, J. Penfold, H. J. Lauter, V. Lauter, and R. Cubitt, Phys. Rev. B **55**, 11 422 (1997).

[53] A. R. Mackintosh and O. K. Anderson, in *Electrons at the Fermi Surface*, edited by M. Springford (Cambridge University Press, Cambridge, England, 1980).

[54] M. Speckmann, H. P. Oepen, and H. Ibach, Phys. Rev. Lett. **75**, 2035 (1995).

[55] H. P. Oepen, M. Speckmann, Y. Millev, and J. Kirschner, Phys. Rev. B **55**, 2752 (1997).

[56] Y. Yafet and E. M. Gyorgy, Phys. Rev. B **38**, 9145 (1988).

[57] A. B. Kashuba and V. L. Pokrovsky, Phys. Rev. B **70**, 3155 (1993); Phys. Rev. B **48**, 10 335 (1993); B. Kaplan and G. A. Gehring, J. Magn. Magn. Mater. **128**, 111 (1993).

[58] Y. Millev, J. Phys.: Condens. Matter **8**, 3671 (1996).

[59] R. Allenspach and A. Bischof, Phys. Rev. Lett. **69**, 3385 (1992).